

*Full Length Research Paper*

# Design and synthesis of nano heterogeneous supported catalysts for olefin polymerization

S. Tajammul Hussain<sup>1\*</sup>, Rafia Naheed<sup>2</sup>, Amin Badshah<sup>2</sup> and Tariq Mehmood<sup>1</sup>

<sup>1</sup>National Centre for Physics, Quaid-i-Azam University, Islamabad, Pakistan.

<sup>2</sup>Department of Chemistry, Quaid-i-Azam University, Islamabad, Pakistan.

Accepted 17 October, 2009

The polymerization of olefins was studied using heterogeneous cobalt nickel (oxide) bimetallic catalyst. The prepared catalyst was subjected to calcination at different temperatures. This treatment results in the formation of different phases with multiple oxidation states. The characterization of the catalyst was carried out by XRD, SEM, EDX, TGA, FTIR and TPR/TPD. The catalytic activity was studied for the polymerization of butadiene gas in toluene, n-hexane and ethanol in a Parr reactor system. The products obtained, were characterized by FTIR, GC/MS, <sup>1</sup>H and <sup>13</sup>C NMR spectroscopy, Laser Light Scattering (LLS) and GPC. The best activity was achieved on the catalyst sample calcined at 1173 K in ethanol solvent. The product contains aliphatic and aromatic carbonyl compounds and polybutadiene terminated by OH group. The GPC and LLS studies indicates that polydispersity of the products are in the narrow range and high molecular weight product. The study reflects that the catalytic reaction conditions, the calcinations temperatures which control the oxidation state, phase of the catalyst and stability of the catalyst are mainly responsible for the change in products selectivity.

**Key words:** Heterogeneous catalysts, bimetallic, olefin polymerization, calcination, solvents, aliphatic, aromatic products.

## INTRODUCTION

Poly-butadiene (BR) is the second largest volume synthetic rubber produced next to styrene butadiene rubber (SBR). The major use of BR is in the tires with over 70% of the polymer produced into treads and side walls. For many polymerization systems, factors that influences the activity/selectivity and conversion of the working catalyst and then the product selectivity have been discussed and revealed that it is the double bonds of butadiene that are key to the polymer formation (Boor, 1979; O'Connor et al., 2007). The butadiene chain attached with the catalyst results in breaking the bond producing a chain growth intermediate which adds to give a long chain polymer product. Keeping into consideration the end product chemistry, the chain is terminated by the addition of OH group containing solvent to accomplish the required goals. Naturally, the molecular characteristics directly in-

directly influence exploitation properties of these polymers. The above mentioned items also relates to the stereo specific polymerization of dienes in the presence of the catalyst complex (a homogeneous catalyst). Modern theories concerning the mechanism of polymerization on Ziegler Natta catalyst explain many effective relationships between catalyst structure, temperature, reagent concentration, catalyst active metal ingredients and the reaction conditions (flow rate, pressure, time of reaction). These affect the polymerization product molecular weight and their chemistry (Saltman, 1977; Galvin, 1989).

To date, the catalyst used for the polymerization of butadiene comprised of an organo-cobalt compound and organo aluminum compound. It must be noted here that in-spite of many workers devoted to Butadiene Polymerization; there are not enough quantitative data in the literature on the influence of catalyst preparation conditions on its activity and stereo specificity and also on the molecular characteristics of the product formed.

The solution polymerization of butadiene is usually car-

\*Corresponding author. E-mail: [dr\\_tajammul@yahoo.ca](mailto:dr_tajammul@yahoo.ca). Tel: +00-92-51-2601003. Fax: +00-92-51-9064-2241.

ried out in hydrocarbon solvents n-Hexane, Cyclohexane and Pentane. These are the most commonly used solvents, the advantage of aliphatic solvents over aromatic solvents are in lower price and lower toxicity. Aliphatic solvents are also superior in the final steps of the industrial process. In contrast to aromatic solvents, aliphatic and cycloaliphatic solvents are considered to be inert (Yu et al., 1993). The use of aromatic solvents results in reduced catalyst activities as already reported by Taube and Sylvester (1996). Another common finding of various studies on the influence of solvent is the decrease of cis-1,4 contents by the use of aromatic solvent (Monteil et al., 2004; Barbotin et al., 1999). In addition to aliphatic and aromatic hydrocarbons, chlorinated aliphatic hydrocarbons and ethers were tested in Nd catalyzed butadiene polymerization. Chlorinated aliphatic hydrocarbons strongly decrease catalyst activity and often yield insoluble polymer gel (Wilson, 1996). Ethers such as THF are catalyst poison.

A series of comparative studies are available in which Nd based catalyst systems were tested in various solvents. Hsieh et al. studied the influence of cyclohexane, n-hexane, n-pentane, chlorinated arenes, toluene, 1-hexane, tetrachloroethylene, and styrene in diene polymerization with the binary system  $\text{NdX}_3 \cdot n\text{D}/\text{AIR}_3$  (Mihir et al., 2009). Duvakina et al. investigated the influence of chlorobenzene, toluene, and cyclohexane on trans-1-4 content. In this study, the binary trans-1,4-specific catalyst system  $\text{NdCl}_3 \cdot \text{TBP}/\text{Mg}$  ( $^{13}\text{C}_4\text{H}_9$ ) ( $\text{C}_8\text{H}_{17}$ ) was used (Duvakina, 2002). For binary Nd ( $\text{O}i\text{Pr}$ ) $_3$  containing catalyst systems, the influence of the solvent heptane, cyclohexane, toluene, dichloromethane was investigated by Dong et al. (2002, 2003). Information about the influence of solvents on ternary Nd systems are available for  $\text{Nd}(\text{N}(\text{SiM}_{33})_2)_3/\text{TIBA}/\text{DEAC}$  (Monteil et al., 2004; Barbotin et al., 1999),  $\text{NdV}/\text{DIBAH}^t/\text{BuCl}$  (Mello et al., 2004)  $\text{Nd}(\text{O}^i\text{Pr})_3/[\text{HNMe}_2\text{Ph}]^+[\text{B}(\text{C}_6\text{F}_5)_4]^-/\text{TIBA}$  (Taniguchi et al., 2005) and  $\text{NdV}/\text{methyl aluminoxane (MAO)}^t/\text{BuCl}$  (Wilson, 1996).

One of the most detailed studies on the influence of solvents is available from Porri et al (Sarasua et al., 2005; Ricci G et al. 1986). In these studies, the Nd carboxylate based systems  $\text{Nd}(\text{isooctanoate})_3/\text{TIBA}/\text{DEAC}$  was used. Porri et al gives the following ranking of the solvents studied: cis-butene > 1-pentene > heptane > (+3% toluene) > toluene > mesitylene > toluene (+7% hexamethylbenzene). The reduction of polymerization rates by aromatics solvents or by the presence of small amounts of aromatic compounds is explained by competitive coordination of monomer and arenes to vacant Nd-sites.

In olefin polymerization, among the best catalysts for the tailoring of the properties of polyolefins are metallocenes. Although metallocene complex can be used in homogeneous form, they are often used in heterogeneous one, that is, they are supported on an insoluble carrier prior to

polymerization, typical support material are silica and alumina, magnesium chloride, zeolites, clays, micelles (Toshima N et al., 1997; Thomas JM et al., 2002). The reasons for the heterogeneous of the metallocene are, for example, slower deactivation of the metallocene, avoidance of reactor fouling, less co-catalyst required, good and uniform polymer morphology, higher polymer density and requirement of the commercial polymerization processes (Song IK et al., 2003).

Methods for heterogenization of the metallocene complex to the support are often divided into three groups. i) Direct immobilization of the metallocene on the support. ii) Immobilization on the support pretreated with methylaluminoxane [MAO] (Bianchini et al., 2002; Denis et al., 2009). iii) Alkylaluminium (Grieken et al., 2003; Minhas et al., 1996) and activation of metallocene with aluminoxane prior to immobilization (Toshima et al., 1997; Song et al., 2003; Knoke et al., 2003).

To-date, the pioneering researches have been making extensive studies in the field of supporting single site catalyst on different supports like  $\text{MgCl}_2$  etc (Xu RW et al., 2006). Heterogeneous catalysts consisting of metals or metal oxides alone or adsorbed on the surface of solid supports are of commercial interest for low pressure polymerization of olefins (Billmeyer, 1984). Common catalyst composition includes oxides of chromium or molybdenum, cobalt and nickel metals, supported on silica, alumina, titania, zirconia or activated carbon (Billmeyer, 1984). The mechanism and kinetics of the mechanism are still largely unknown although many proposals like those made for Ziegler-Natta polymerization have been presented.

To the best of our knowledge there are only few reports in the field of heterogeneous bimetallic catalyst systems having different oxidation states and phases used for polymerization studies. This study extensively report the polymerization of Butadiene using heterogeneous metal catalysts coupled with the effect of different solvents and calcination temperature on the product selectivity.

We have found an interesting aspect from this study that by varying the reaction parameters and catalyst calcination temperature we can direct the polymerization products selectivity towards aliphatic/aromatic and trans or cis product formation. The kinetic parameters of the reaction are also studied and reported here. On the basis of our findings we postulated a mechanism for the formation of different molecular weight polymer products with very narrow polydispersity.

## Experimental

### Materials

$\text{Co}(\text{NO}_3)_2 \cdot 6\text{H}_2\text{O}$  purity of > 99% of FLUKA,  $\text{Ni}(\text{NO}_3)_2 \cdot 6\text{H}_2\text{O}$  Purity of > 98% of FLUKA, Citric Acid Purity of > 99.5% used as a reducing agent. Ammonium hydroxide ( $\text{NH}_4\text{OH}$ ) (35% of Merk) was

**Table 1a.** Preparatory Variables and EDX analysis.

Catalyst Designation	Amount of Cobalt salt	Amount of Nickel salt	Citric acid	EDX Analysis		
				%Co	% Ni	% O <sub>2</sub>
Ni:CO (O <sub>x</sub> )	3 g	3 g	10g	37.0	38.0	25.0

**Table 1b.** Particle size calculated from Scherer EQUATION, specific surface AREA and BET.

Catalyst designation	Particle Size (nm) 673K	Specific surface area/volume (microns) 873K	Particle size (nm) 1173K	Specific surface area/volume (microns) 1173K	BET surface area analysis		
					m <sup>2</sup> g <sup>-1</sup> (673)K	m <sup>2</sup> g <sup>-1</sup> (873)K	m <sup>2</sup> g <sup>-1</sup> (1173)K
Ni:Co(O <sub>x</sub> )	146.0	0.99	160.0	0.95	31	26	20

used to enhance the adsorption of metal on solid support. Freshly dried Toluene of Merk, n-Hexane Analytical Grade of Merk and absolute Ethanol along with Butadiene gas of purity of 99.999% were used in the study.

#### Catalyst preparation

The catalysts were prepared using citrate route of sole gel. Citric acid was used as a reducing agent and ethanol as a solvent. Cobalt, Nickel nitrate and citric acid mole ratio of 1: 4 in 80 ml ethanol was mixed for 30 min at 353 K. The resulting slurry was dried at 473 K for 2 h. The resulting solid was divided into three portions and calcined at 673, 873 and 1173 K for 6 h to obtain different oxidation states of Cobalt/Nickel oxide bimetallic catalyst.

The preparatory variables, catalyst compositions, specific and BET surface area and EXD analysis of the prepared samples are presented in Tables 1a and b.

#### The catalyst characterization

The morphologies of the support, the synthesized catalysts were examined by Phillips scanning electron microscope (SEM) XL-30ESEM FEG, equipped with an energy dispersive X-ray spectrometer (EDX). The samples were prepared according to the procedure reported by Huang et al. (2004). XRD (Phillips PW 3040/60 X Pert Pro) powder diffractometer was used for analysis, using nickel filtered copper K alpha radiations with generator setting of 40 KeV. The diffraction patterns were recorded in the range, 5° ~70°. The peak identification was accomplished in comparison with ASTM standard diffraction data file. BET surface area of all the samples were determined by nitrogen physisorption using a Micromeritics ASAP 2010. The samples were degassed at 155°C for 3 h before the experiment. The thermal decomposition behaviors of the samples were studied by Thermogravimetric analysis (TGA) and differential thermal analysis (DTA) on a Mettler TGA/SDTA 851 in oxygen environment. Temperature-programmed reduction (TPR) studies were carried out with TPDRO 1100 Series Thermo Electron Corporation system. The accuracy was ± 5°C. The Infrared (IR) spectra of the catalysts and product were obtained on Bio-Red Excalibur FTIR Model 3000 MX as KBr pellet and as NaCl cell respectively. The <sup>1</sup>H and <sup>13</sup>C-NMR spectra of polymer were recorded on a Bruker 300 MHz instrument, using deturated chloroform CD<sub>3</sub>OD as solvent. The GPC analysis was performed using Perkinelmer Injector Detector L3350 equipped with RI Monitor. All the samples were referenced to standard. Laser Light Scattering

(LLS) of the products were performed using a commercial light-scattering spectrometer (ALV/SP-150 equipped with an ALV-5000 multi-τ digital time correlator) was used with a solid-state laser (ADLAS DPY 425II, output power ≈ 400 mW at λ = 532 nm) as light source. For each sample, four concentrations ranging from 2.0 × 10<sup>-3</sup> to 8.00 × 10<sup>-3</sup> g/ml were prepared by dilution. All polymer solutions were filtered by using a 0.50 μm Whatman filter in order to remove dust completely.

Analysis of the exit gasses and oily samples were carried out using on line GC/MS 6890N Egilent Technology USA. The poropak Q column was used for GC analysis. Before the analysis the GC was calibrated using standard mixtures of hydrocarbons aliphatic/aromatics products supplied by BOC, UK.

#### Butadiene polymerization

For each experiment 2.5 g of catalyst was loaded inside the SS microreactor (Figure 1) using ethanol, n-hexane and toluene in three different experiments with catalyst samples calcined at 673, 873 and 1173 K. The system was flushed with argon to ensure complete removal of air from the microreactor and then butadiene at 50 ~ 60 psig (pounds per square inch) pressure at a flow rate of 40 - 50 mls/min was injected into the microreactor with continuous stirring. The temperature of the reaction was raised to 130°C in increment of 5°C. The reaction temperature was maintained at 130°C for 2 h. The catalytic reaction was monitored with continuous injecting the sample in to on line GC/MS, when the product becomes stabilized the reaction was stopped and the resultant mixture was analyzed using <sup>1</sup>H-NMR and <sup>13</sup>CNMR along with GC/MS, FTIR, GPC and LLS (Laser Light Scattering).

Blank experiments were also carried out and the product obtain was analyzed by NMR and GC/MS but no appreciable peak was obtain.

## RESULTS AND DISCUSSION

### Characterization of catalysts

SEM micrographs of the samples calcined at different temperatures are presented in Figures 2a, 2c and 2e (Fresh Catalysts). No open pore structures can be seen on Fresh samples calcined at 673 and 873 K. The sample calcined at 1173 K shows irregular pore structure.

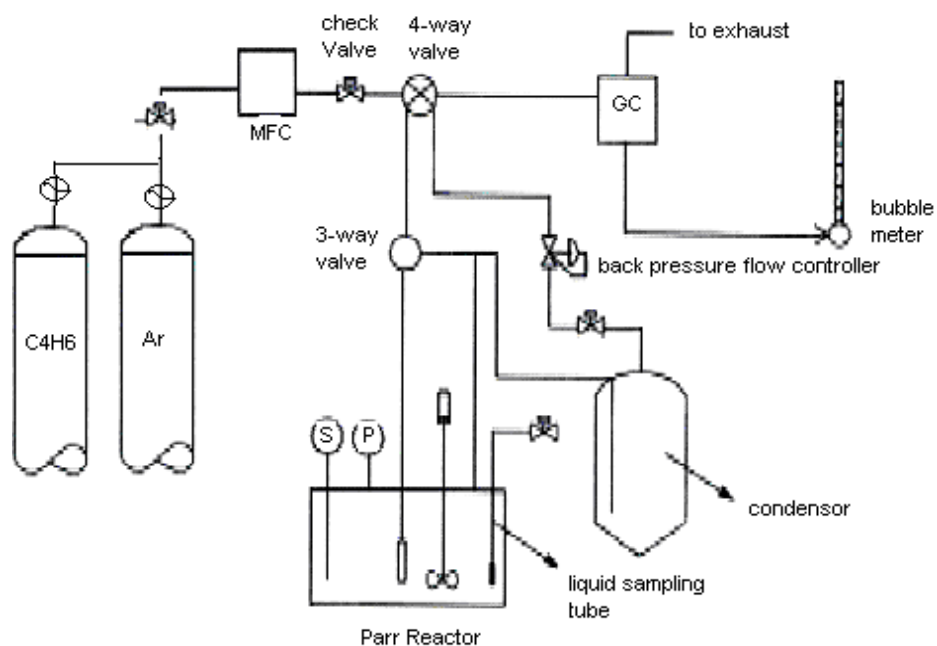


**Figure 1.** Catalytic activity test system.

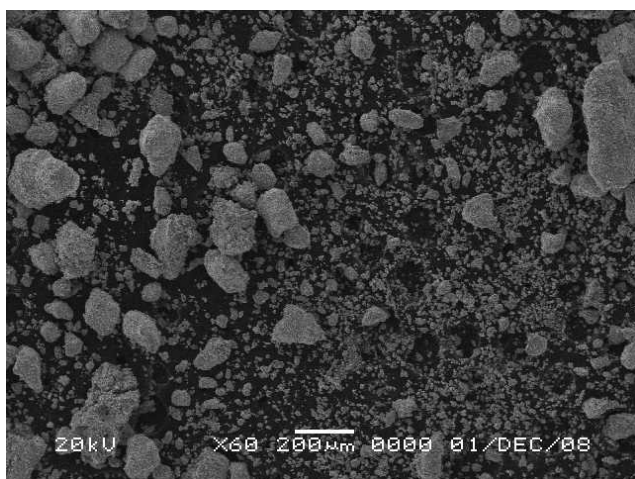


**Figure 2a.** SEM analysis of the prepared catalyst system (Fresh, calcined at 673 K).

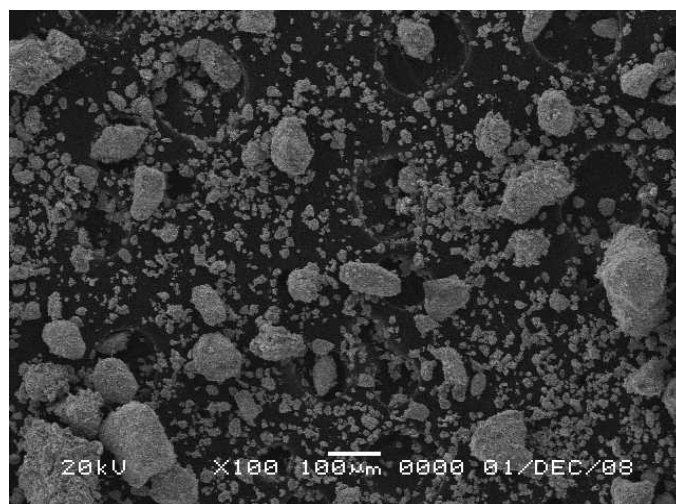


**Figure 2b.** SEM analysis of the prepared catalyst system (spent calcined at 673K).

The packing order seen on these samples could be due to geometrically well defined channels of the oxide formed and such structures are fairly stable. The SEM analysis performed on the spent catalysts (Figure 2b, 2d and 2f) does support our argument, where the particle size, characteristics and the nature of the catalytic active sites changes appreciably.

The adsorption-desorption curve shown in Figure 3 support our argument presented above where the hysteresis structure of the catalysts reflects the formation of channel-

ing within the sample pores, these channeling changes the adsorption and desorption chemistry of the catalyst during the polymerization reaction and consequently results in the highest specific surface area and excellent polymerization properties.

#### Catalyst characterization using XRD

The XRD of the samples calcined at different tempera-

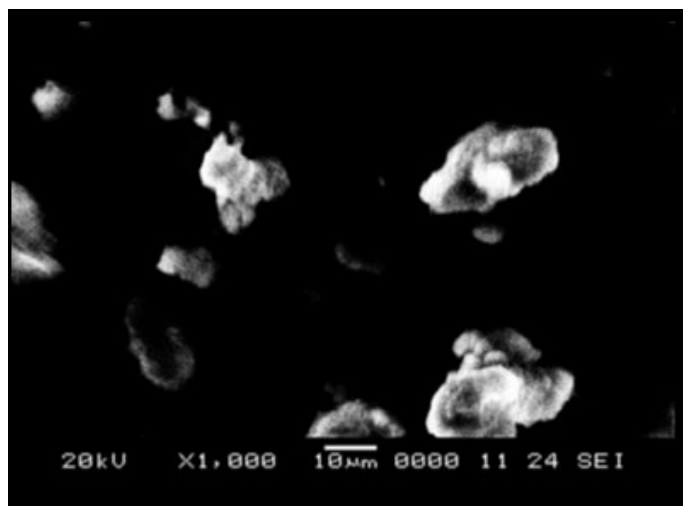


**Figure 2c.** SEM analysis of the prepared catalyst system (Fresh, calcined at 873K).

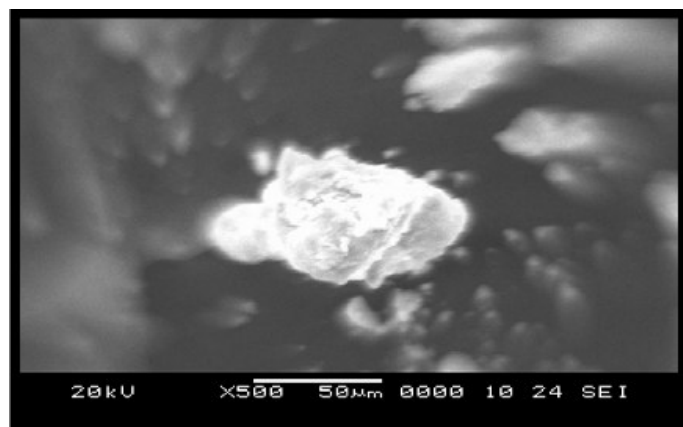


**Figure 2d.** SEM analysis of the prepared catalyst system (spent calcined at 873K).

tures are presented in Figures 4a and b. The study of the XRD data reveals crystalline characteristics of the catalyst samples calcined at 673 and 873 K, because of narrower peak width in comparison of the sample calcined at 1173 K. The particle size of the calcined and prepared catalyst samples are calculated from Scherrer equation (with a standard deviation of  $\pm 10\%$  because of limitation of XRD particle size calculation  $< 100$  nm). BET and specific metal surface area of the catalysts is calculated using procedures described by Takehira et al. (2004) presented in Table 1b. Study of the peak intensity of the catalyst samples calcined at 1173 K indicates phase transition from octahedral  $\text{Co}_3\text{O}_4$  to tetrahedral of  $\text{CoO}$  and  $\text{Ni}$  shift to  $\text{Ni}^{+2}$  states (Narayan et al., 2006; Jin et al., 1991; Huang et al., 2003). Whereas, only one phase of  $\text{Ni}$  and  $\text{Co}$  is seen on the samples calcined at 673 and 873

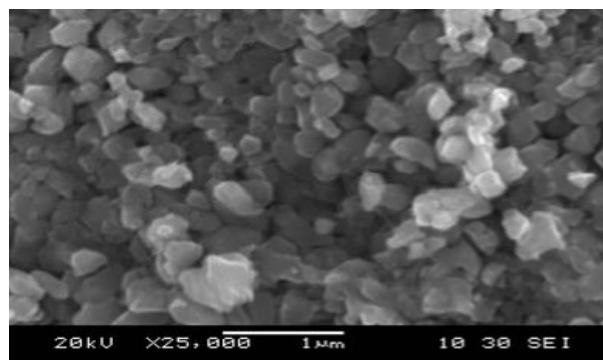


**Figure 2e.** SEM analysis of the prepared catalyst system (Fresh, calcined at 1173 K).

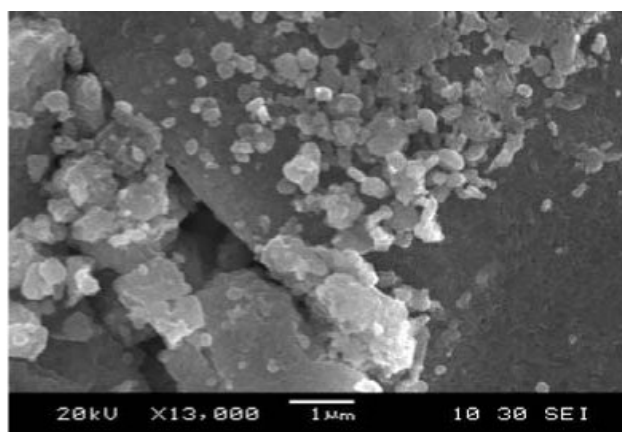


**Figure 2f.** SEM analysis of the prepared catalyst system (spent calcined at 1173K).

K. The peak broadening and low intensity on the catalyst calcined at 673 and 873 K reflects the amorphous nature of the prepared system. The 1173 K calcined sample shows electronic interaction of  $\text{Ni}:\text{Co}(\text{O}_x)$ . The increase in particle size also confirms the high crystalline nature of the material. This is a direct indication of the effect of calcination temperature on the catalyst oxidation states.

The reduction degree for the catalyst calcined at 673, 873 and 1173 K were calculated using the procedure described by Jin et al. (1991) and Huang et al. (2003) in ethanol, n-hrxane and toluene solvents, respectively. For samples calcined at 1173 K, the reduction degree ( $\alpha$ ) comes out to be 0.73 which is much higher in comparison with the catalyst calcined at 673 and 873 K ( $\alpha = 0.23$  and 0.27 respectively). This is an agreement with the diffusion problems observed by Serra et al. (2005).

### Catalyst characterization using TGA

Thermodynamic parameters were calculated from TGA

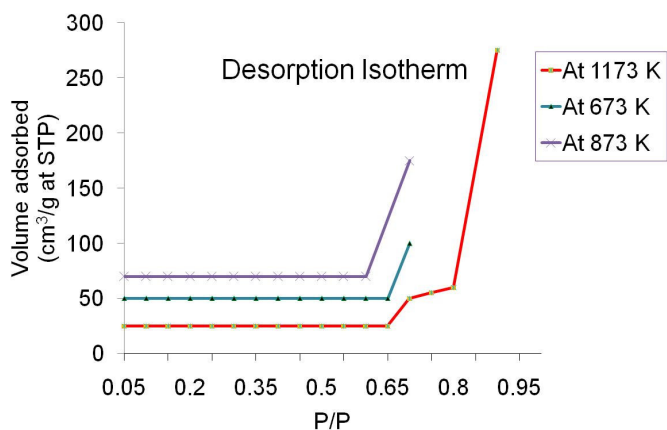


Figure 3. Adsorption-Desorption Isotherm of sample (Ni:Co(O<sub>x</sub>)).

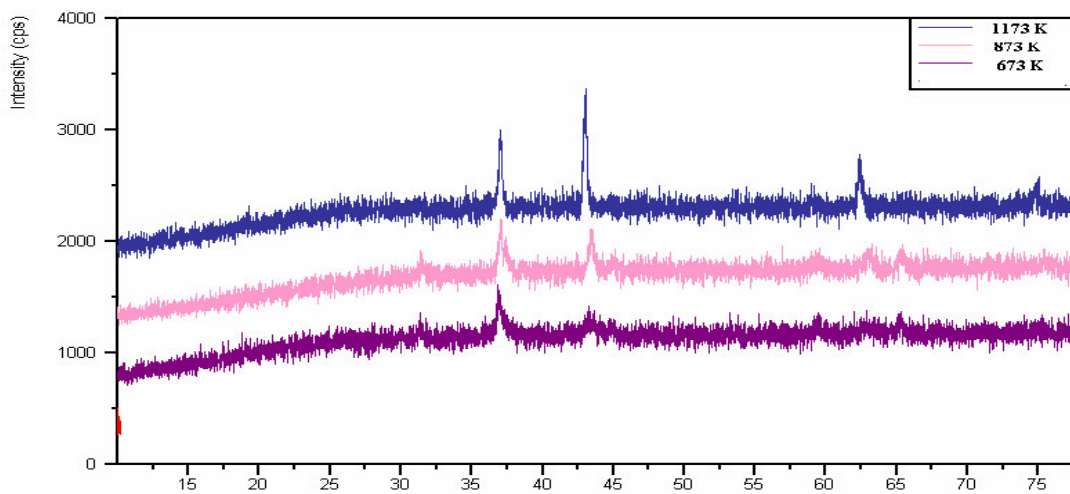


Figure 4a. XRD analysis of the catalyst system (Fresh).

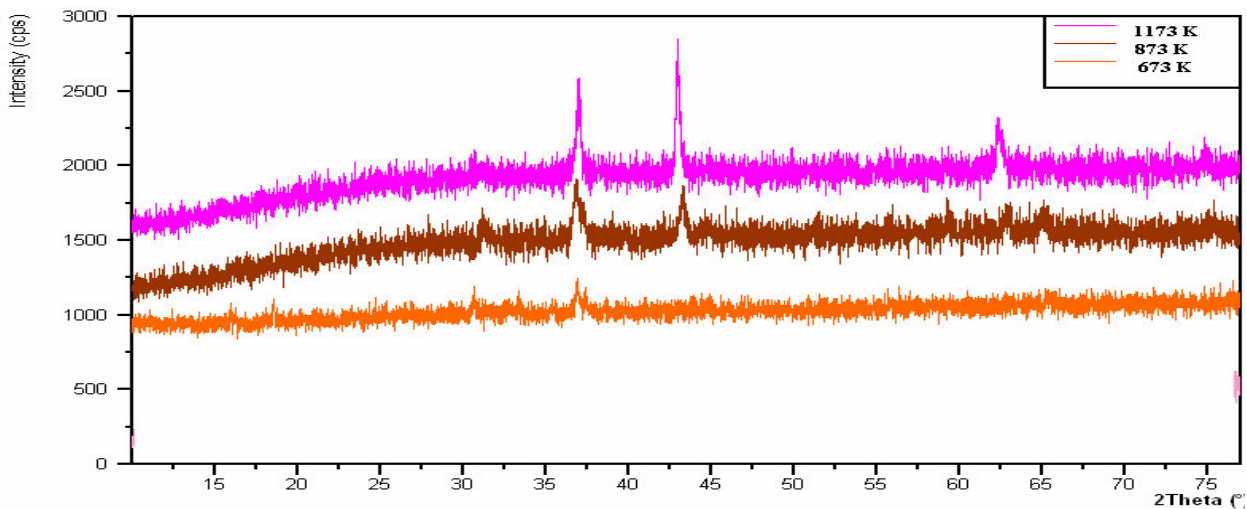


Figure 4b. XRD analysis of the catalyst system (Spent).

**Table 2.** Thermodynamics Parameters calculated from TGA data.

Catalyst designation	$\Delta S$ (Kcals/mol)			$\Delta H$ (Kcals/mol)			$E_a$ (Kcals/mol)		
	1173K	873K	673K	1173K	873K	673K	1173K	873K	673K
Ni:Co(O <sub>x</sub> )	-210.52	-258.81	-271.28	18.79	9.90	5.86	10.47	17.71	22.63

$E_a$  = Activation Energy of catalytic reaction.

$\Delta H$  = Heat of reaction.

$\Delta S$  = Disorderness of the catalytic reaction.

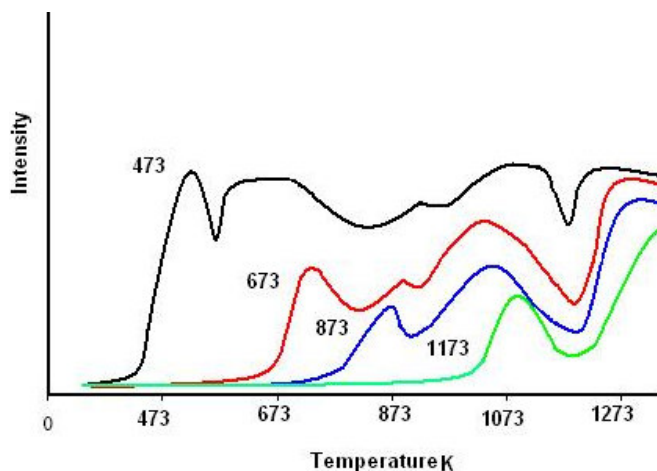


**Figure 4c.** TPD studies of the prepared system calcined at 473, 673, 873 and 1173

studies using in house developed software and are presented in Table 2. The thermodynamic parameters suggest that the formation of Ni:Co(O<sub>x</sub>) bimetallic electronically modified geometry on the sample calcined at 1173 K are in comparison with other catalysts because of the changes induced within the catalyst lattices as can be observed with the change in entropy, heat of reaction and activation energy. These higher oxidation states of Ni:Co(O<sub>x</sub>) changes the reaction chemistry during the polymerization reaction. It produces an extra amount of energy because of higher oxidation states which results in increase in acidic nature of the active sites. This makes the reaction exothermic and its activation energy is decreased. This is a direct reflection of the presence of electronically modified active sites within the catalyst matrix, which results in increased catalyst activity, product selectivity and % conversion. The EDX analysis presented in Table 1a reflects the changes in the reaction chemistry, where the Nickel and Cobalt concentration on this catalyst comes out to be 38 and 37%, respectively, consequently, the major contribution in the catalyst behavior comes from mixed Co:Ni(O<sub>x</sub>) bimetallic phase, geometry, mechanical strength and particle shape. It is our observation that edges and corners of the catalyst particles have an important role to play during the poly-

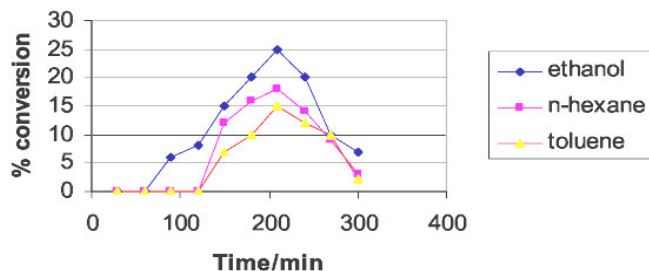
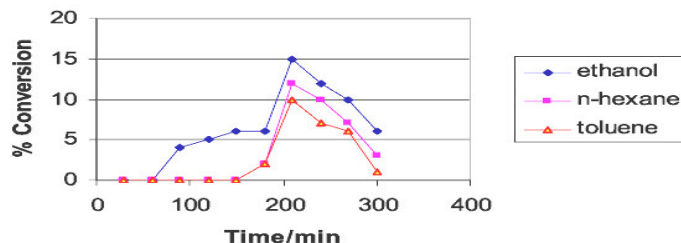
merization process, where the adsorption/desorption chemistry stoichiometry changes, resulting in the production of polymeric products.

### The TPD study

The Temperature Programmed Reduction/Desorption equipment is equipped with 273 -1273 K programmable temperature furnace. Each sample (50 mg) was first heated at 673 K in an argon flow (80 cm<sup>3</sup>/min) for 3 - 4 h to remove all the surface impurities. The sample was then heated in a vol %H<sub>2</sub>/Ar flow (80 cm<sup>3</sup>/min) from 673 to 1173 K at a rate of 5 K min<sup>-1</sup> and maintained at 1173 K until reduction process was finished. The TPD was performed (presented in Figure 4c) in pure hydrogen with a flow rate of 80 cm<sup>3</sup>/min. The temperature was raised to 673 K from room temperature at 1 K mn<sup>-1</sup> up to 673 K. They were isothermally maintained at this temperature for 4 h. The samples were then cooled to room temperature in the hydrogen flow and heated at a rate of 10 K/min to 1123 K. The hydrogen desorption was detected with TCD detector. For the Hydrogen chemisorption, the samples were reduced under the same condition described above. After reduction, the chemisorbed hydrogen was removed in the stream of 30 ml/min of He for 30 min at 683 K. The sample was subsequently cooled to 303 K in the He stream. The chemisorbed hydrogen was analyzed at 303 K. The nickel and cobalt surface area was calculated assuming a stoichiometry of one hydrogen molecule per two surface atoms and an atomic cross sectional area of 6.49 x 10<sup>-20</sup>m<sup>2</sup>/Ni, Co atoms. The reducibility of all the samples was estimated by TPR, considering its initial reduction temperature obtained from the literature (Takehira et al., 2004). Our goal was to confirm the degree of reduction ( $\alpha$ ) observed by XRD on our catalysts. The initial reduction temperatures values are 680 K for NiO, 693 K for CoO, 786 K for Ni and Co(O<sub>x</sub>), 1054 K. This confirms that the interaction between NiO:Co(O<sub>x</sub>) leads to the formation of bimetallic NiO:Co(O<sub>x</sub>) sites. To obtain information about their active sites, temperature programmed desorption of hydrogen was performed on all the catalysts samples. The mechanism of adsorption/desorption of hydrogen are extremely complex (Cesteros et al., 2000; Kowalski et al., 2003) especially when dealing with bimetallic catalyst system. The is because

**Table 3.** Interpretation of FTIR Spectra of the fresh (F) and spent (S) Catalysts.

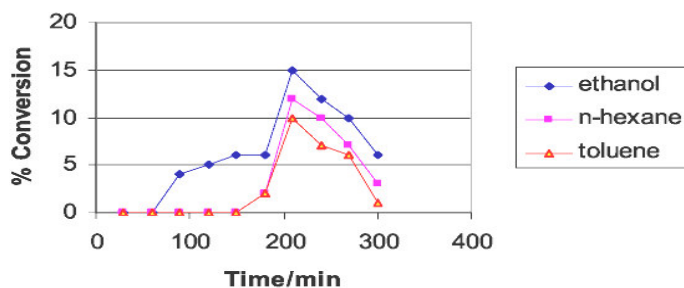
Catalyst	C-O-C	O    C-C	In plane Pri-alcoholic C-OH	Second Ary-CH <sub>2</sub> OH	C = C	C=O	- OH
Ni:Co(O <sub>x</sub> )(F)	----	----	----	----	----	----	-
Ni:Co(O <sub>x</sub> )(S)	1110	1123	1274	1384	1647	1730	3456

**Figure 5a.** Conversion time plot of the catalyst Ni:Co(O<sub>x</sub>) calcined at 1173 K.**Figure 5b.** Conversion time plot of the catalyst Ni:Co(O<sub>x</sub>) calcined at 873K.

phenomena related to the interaction between different active phases can interfere. TPD data shows two peaks in the lower temperature region with a maxima at 450 - 510 K and 530 - 620 K, respectively for all catalysts and one peak at the temperature region (with maxima at 823 - 856) for samples Ni:Co (O<sub>x</sub>) calcined at 1173 K. The low temperature TPD profile has been associated with different adsorption states of the hydrogen on bimetallic catalysts (Cesteros et al., 2000; Kowalski et al., 2003). It is attributed to the occurrence of high temperature peaks to hydrogen spillover taking place during high temperature treatment of our catalysts. We also suggest here taking into consideration the discussions presented above that the high temperature peak is associated with other adsorption states of hydrogen (due to a difference in morphology and changes in particle size). Another point worth considering here is that higher metallic area attained on the supported catalysts results in the lower adsorption peaks of hydrogen and especially due to the presence of specific active oxidation states induced in the system by different calcinations temperatures. This is the reason why the changes in catalytic activity/selectivity and product distribution, takes place on our system.

### The FTIR studies

The FTIR studies presented in Table 3 on fresh and spent catalysts shows a sharp band at 1384 cm<sup>-1</sup> and a broad band at 3456 cm<sup>-1</sup> on the spent catalyst. These bands are due to CH<sub>2</sub>OH as adsorbed species. The absorption band in the range of 1647 cm<sup>-1</sup> indicates the presence of C=C group, the sharp and characteristic

**Figure 5c.** Conversion time plot of the catalyst Ni:Co(O<sub>x</sub>) calcined at 673K.

peak of carbonyl group C=O is present at 1730 cm<sup>-1</sup>. The weak and medium intensity of C-O-C is present in the range of 1110 cm<sup>-1</sup>, on the surface of spent catalyst. This indicates that whole polymerization process takes different interaction routes on different types of active sites due to different oxidation states and phases of Ni and Co as confirmed by TGA and XRD studies. The FTIR data of fresh (F) and spent (S) catalyst before and after catalytic reaction is presented in Table 3, which supports our findings.

### Catalytic activity

The conversion-time plot presented in Figures 5a - 5c for the polymerization process is transformed in to first order plots while Figure 6 reveals that polymerization rate decreases in order ethanol>n-hexane>toluene. The maximum conversion is achieved on the catalyst sample calcined at 1173 K (Figure 5a). On the basis of the re-

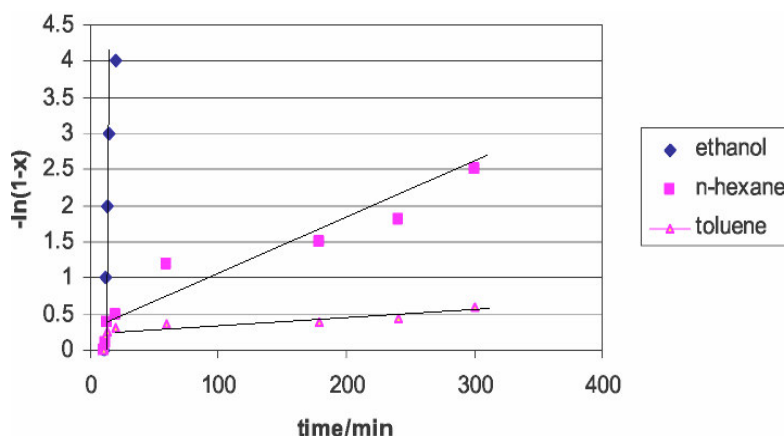


**Figure 6.** The conversion time plot of figure (4, a-c) is transferred into first order plots  $[-\ln(1-x)$  vs time] for the catalyst Ni:Co(Ox) calcined at 673, 873 and 1173 K.

results presented in Figure 6, a linear dependency is only obtained for the polymerization in ethanol. The respective first-order plots polymerization of n-hexane and toluene are curved. The deviation from the respective straight lines is more pronounced in n-hexane and in toluene. On the basis of this evidence only the polymerization in ethanol is in compliance with the first order requirement for a living polymerization (Huang et al., 2003). Due to deviation from the first order dependencies, the polymerization in n-hexane and toluene do not comply with the requirement. From the argument reported by Huang et al. (2003); Serra et al. (2000); Cesteros et al. (2000); Kowalski et al. (2003); Penczek et al. (2002), it can be concluded that irreversible chain termination reactions occur in n-hexane and toluene.

In order to quantitatively compare catalyst activities in ethanol, n-hexane and toluene, catalyst turn over frequencies (TOF) were calculated from the time conversion plots given in figures 5(a-c). The following orders of TOF values were determined: 7620 h<sup>-1</sup> for ethanol > 3452 h<sup>-1</sup> for n-hexane > 1650 h<sup>-1</sup> for toluene. From the ratios of TOF values the relative apparent concentration of active species can be estimated: for ethanol >1, for n-hexane >0.21, for toluene >0.11. The reduction of active Ni:Co(Ox) sites in n-hexane and in toluene can be quantitatively explained on the basis of competitive coordination between butadiene and n-hexane and toluene solvents to active Ni:Co(Ox) oxidation states which constitute active catalytic centers for this process. As n-hexane and toluene have more or less similar Lewis basicity, the lower polymerization activity in both cases is a hint of an additional reduction of active sites by irreversible chain termination.

The higher product selectivity achieved in case of ethanol could be ascribed due to the characteristic surface properties of the catalyst, leading to sufficiently

coverage with weakly bound hydrogen which diverts the reaction towards the formation of aliphatic products at lower temperature. The catalyst calcined at higher temperature tilted more towards strongly bound hydrogen, thereby increasing the concentration of surface intermediates, thus producing aromatic hydrocarbons. At weakly bound hydrogen crystallization is not favored. On the other hand the strong bonded hydrogen increases the hydrogen/intermediate ratio and thus producing enough hydrogen enriched species to give the aromatic products. We also propose here at lower temperature the crystallinity of the catalyst particles also contribute towards the shift in product formation. The metal surface area availability could be another cause.

From the activity data we can also suggest that the temperature of calcinations of our catalyst system strongly influence the molecular weight distribution of the resultant polymers. When the catalyst is calcined at 673 and 873 K respectively the resultant catalyst were found not significantly active for butadiene polymerization. On the contrary the catalyst pretreated at 1173 K was found active because of the uneven particles shape as can be seen in SEM study. A particularly important feature of heterogeneous catalyst in case of polymerization is its ability to give uneven particle size and geometry. As indicated in SEM study of the Ni:Co(Ox) catalyst, calcined at 1173 K is the formation of channels and uneven surface, consequently the polymerization is taking place outside and inside of the catalyst almost simultaneously that's why this catalyst is highly productive due to good morphology and high bulk density. This argument confirms that, this type of catalyst morphology can be replicated throughout catalyst preparation and treatment. An important factor in the polymerization process is the particle size which generates extra amount of thermal energy during the polymerization process to proceed.

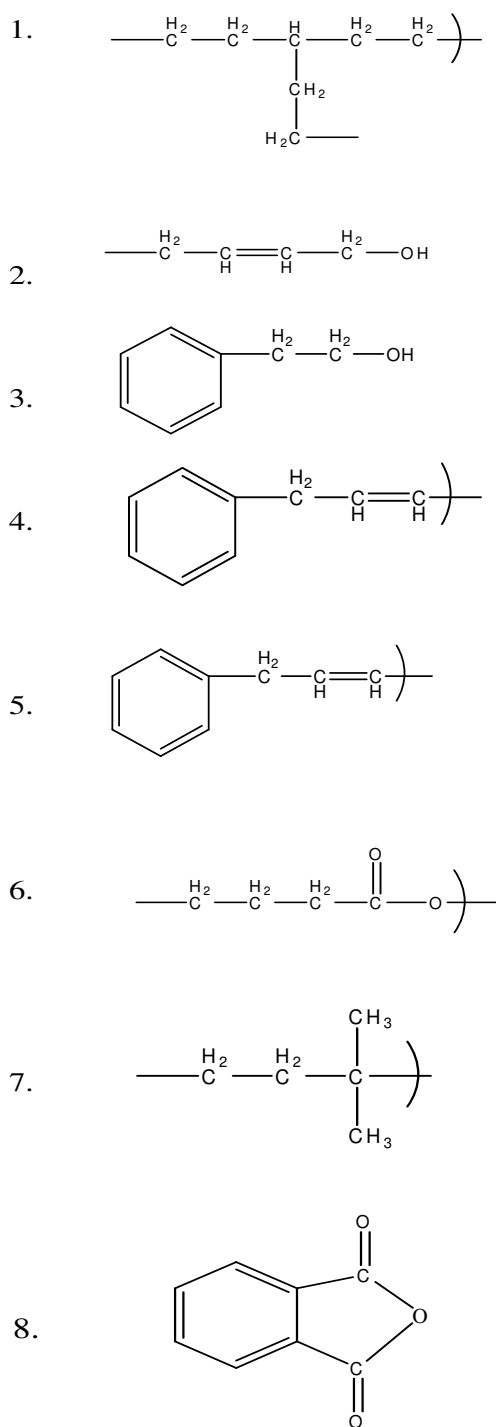


Figure 7. The Microstructures.

The carbon mass balance of the process was maintained during the catalytic polymerization studies. Conversion and activity were calculated using the following procedure: Conversion (%): [moles of 1,4 Butadiene consumed] x 100 [moles of 1.4 Butadiene charged]; Acti-

vity (%): [moles of one product of reaction] x 100/[moles of 1,4 Butadiene consumed].

### Characterization of products

The microstructure of Butadiene Polymerization product was determined by IR spectroscopy (Figures 7 and 8). The following peaks were used for quantitative determination of polymer structure: 723 ~ 760  $\text{cm}^{-1}$  is due to long chain band. The vinyl loop for ( $\sigma$  (cis-R-CH=CR-H)  $\int$  cis-1-4,  $\sim$  =0.192), 912  $\text{cm}^{-1}$  ( $\sigma$  (R-CH=CH-H),  $\int$  1, 2,  $\sim$  =1.0), 965  $\text{cm}^{-1}$  ( $\sigma$  (trans-R-CH=CR-H),  $\int$  trans-1, 4,  $\sim$  =0.769). The aromatic absorption band is present in 1580~1600  $\text{cm}^{-1}$ . The polymeric H-bonding is found in 3400 ~ 3441  $\text{cm}^{-1}$ ,

The absorption at 3150  $\text{cm}^{-1}$  is due to stretching of =C-H. The characteristic carbonyl peak is present at 1730  $\text{cm}^{-1}$  as shown in Figure 8. The validity of the Lambert-Beer law was assumed.

Polybutadiene which are predominantly of 1, 4 microstructure show two major signals of  $^{13}\text{C}$  at 27.2 ~ 27.4 and 32.5 ~ 32.7 ppm corresponding to cis and trans methylene carbons next to 1,4 units respectively. A high vinyl contents, a methylene carbon line at 30.97 ppm has been assigned. The peaks assigned at 42.03 ~ 44.51 ppm is for 1, 4-v-1, 4 CH (Krajewski-Bertrand et al., 1996). When polymerization is carried out in ethanol solvent, we can get the microstructures of aliphatic and aromatic carbonyl compounds. Figure 9 shows the signals at 167.8, 128.81, 130.9 and 132.43 ppm of  $^{13}\text{C}$  and 7.53, 7.76 ppm of  $^1\text{H}$  are the specific signals of microstructure of phthalic anhydride (Brandolini et al., 2000) as also shown in the MS results presented in Table 4. The fragmentation pattern of different monomers support our argument presented above.

Monomer conversion was determined gravimetrically. For this purpose, samples were taken and weighed (still containing solvent and monomer). The weight of the samples was determined again after polymerization had been short stopped with ethanol and after residual solvent has been removed by vacuum drying at 338 K. Kinetic parameters of polymerization were calculated from product molecular mass plotted vs time of polymerization and monomer and catalyst concentration according to Gilbert et al. (1983) and Duan et al. (2009).

The  $^{13}\text{C}$ ,  $^1\text{H}$ - NMR and GC/MS data of the synthesized compounds showed that microstructures obtain were of three different types: 1) Saturated hydrocarbon alkanes; 2) Unsaturated polymeric alkenes with OH group and C=O group; 3) Aromatic carbonyl compounds.

### Characterization of product using laser light scattering (LLS)

A commercial light-scattering spectrometer (ALV/SP-150

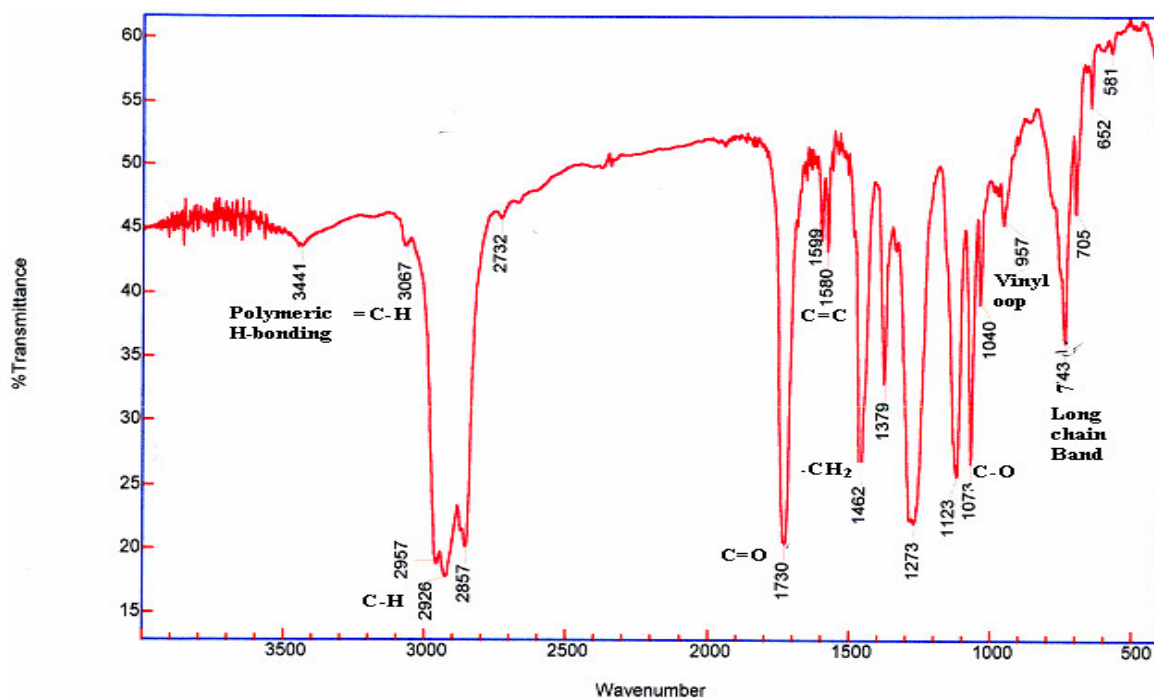


Figure 8. FTIR spectra of the Product.

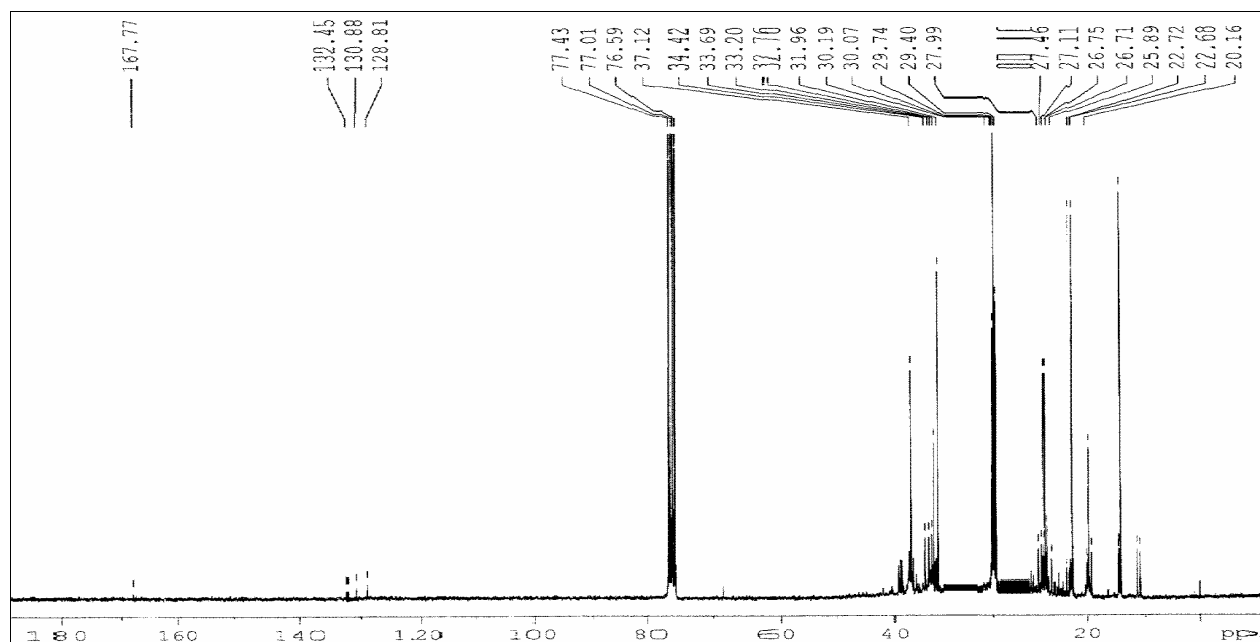


Figure 9. <sup>13</sup>C-NMR spectra of the Product.

equipped with an ALV-5000 multi- $\square$  digital time correlator) was used with a solid-state laser (ADLAS DPY 425II, output power  $\square$  400 mW at  $\square$  = 532 nm) as light source. The incident beam was vertically polarized with respect to the scattering plane. For static LLS, the

instrument was calibrated with toluene to make sure that there has no angular dependence in the scattering angle of 20° - 150° from toluene. The detail of the LLS instrumentation and theory can be found elsewhere (Pecora et al., 1976; Chu, 1991). All the measurements were carried out

**Table 4.** Mass Spectrometric analysis of the products.

Empirical formula	M/2	Empirical formula	M/2	Empirical formula	M/2	Empirical formula	M/2	Empirical formula	M/2
C <sub>8</sub> H <sub>5</sub> O <sub>3</sub> <sup>+</sup>	149	C <sub>3</sub> H <sub>7</sub> <sup>+</sup>	43	C <sub>11</sub> H <sub>23</sub> <sup>+</sup>	155	C <sub>18</sub> H <sub>35</sub> O <sup>+</sup>	267	C <sub>23</sub> H <sub>45</sub> O <sup>+</sup>	337
-	-	C <sub>4</sub> H <sub>9</sub>	57	C <sub>12</sub> H <sub>24</sub> <sup>+</sup>	168	-	-	-	-
C <sub>8</sub> H <sub>4</sub> O <sub>2</sub> <sup>+</sup>	132	C <sub>6</sub> H <sub>13</sub> <sup>+</sup>	85	C <sub>13</sub> H <sub>27</sub> <sup>+</sup>	183	C <sub>19</sub> H <sub>37</sub> O <sup>+</sup>	281	C <sub>24</sub> H <sub>47</sub> O <sup>+</sup>	351
C <sub>7</sub> H <sub>5</sub> O <sub>2</sub> <sup>+</sup>	121	C <sub>7</sub> H <sub>13</sub> <sup>+</sup>	97	C <sub>14</sub> H <sub>29</sub> <sup>+</sup>	197	C <sub>20</sub> H <sub>39</sub> O <sup>+</sup>	295	C <sub>25</sub> H <sub>47</sub> O <sup>+</sup>	363
C <sub>8</sub> H <sub>10</sub> O <sup>+</sup>	122	C <sub>8</sub> H <sub>15</sub> <sup>+</sup>	111	C <sub>15</sub> H <sub>27</sub> <sup>+</sup>	207	C <sub>21</sub> H <sub>40</sub> O <sup>+</sup>	308	C <sub>27</sub> H <sub>51</sub> O	391
C <sub>7</sub> H <sub>4</sub> O <sup>+</sup>	104	C <sub>9</sub> H <sub>17</sub> <sup>+</sup>	125	C <sub>15</sub> H <sub>29</sub> O <sup>+</sup>	225	-	-	-	-
-	-	C <sub>10</sub> H <sub>21</sub>	141	-	-	-	-	-	-
-	-	-	-	C <sub>17</sub> H <sub>33</sub> O <sup>+</sup>	253	C <sub>22</sub> H <sub>42</sub> O <sup>+</sup>	322	-	-

**Table 5.** Summary of the static laser light-scattering (LLS) results.

Catalyst samples	(M <sub>w</sub> ) 10 <sup>-5</sup> (g/mol)	<R <sub>g</sub> > (nm)	A <sub>2</sub> 10 <sup>4</sup> (mol.mL/g <sup>2</sup> )
Calcined at 1173 K	7.15	75.00	2.76
Calcined at 873 K	4.40	55.40	4.35
Calcined at 673 K	2.52	36.15	6.50

**Table 6.** GPC analysis of the product stream.

Samples	M <sub>w</sub>	M <sub>n</sub>	M <sub>w</sub> /M <sub>n</sub>
Calcined at 1173K	1454	1352	1.0757
Calcined at 873K	1225	1210	1.0985
Calcined at 673K	1180	1071	1.1010

at 25 ± 0.1 °C and are presented in Table 5. The angular dependence of the excess absolute time-averaged scattered intensity, known as the excess Rayleigh ratio, R<sub>vv</sub>(q), of a dilute polymer solution was measured. For a dilute polymer solution at a relatively low angle θ, R<sub>vv</sub>(q) can be expressed as (Zimm, 1948).

$$\frac{KC}{R_{vv}(q)} \approx \frac{1}{M_w} \left( 1 + \frac{1}{3} \langle R_g^2 \rangle q^2 \right) + 2A_2C \quad (1)$$

Where;  $K = \frac{4\pi^2 n^2 (dn/dc)^2}{N_A \lambda_0^4}$  and  $q = \frac{4\pi}{\lambda_0} \sin(\theta/2)$  with N<sub>A</sub>, dn/dc, n and λ<sub>0</sub> being Avogadro's number, the specific refractive index increment, the solvent refractive index, and the wavelength of the light in vacuo, respectively. M<sub>w</sub> is the weight average molar mass; A<sub>2</sub> is the second virial coefficient; and  $\langle R_g^2 \rangle_z^{1/2}$  is the root-mean square z-average radius of gyration of the polymer chain. Refractive index increment of (~0.105 ml/g) for the polymer was measured by a high-precision differential refractometer (Wu, 1994), which enables us to measure dn/dc

and the scattered wavelength under identical experimental condition, so that the wavelength correction was eliminated. It is vital in static light scattering to have a precise value of differential refractive index increment, dn/dc, because the measured M<sub>w</sub> is proportional to (dn/dc)<sup>-2</sup>. The results of the experiment are presented in Table 5 and Figure 10.

Figure 10 shows a typical Zimm plot of catalyst samples in THF at 25 °C, where a 0.50 μm filter was used and C range from 2.00 x 10<sup>-3</sup> to 8.00 x 10<sup>-3</sup> g/mL. On the basis of equation 1, we have calculated the values of M<sub>w</sub>, <R<sub>g</sub>> and A<sub>2</sub> respectively from [KC/R<sub>vv</sub>(θ)]<sub>θ→0, c→0</sub>, [KC/R<sub>vv</sub>(θ)]<sub>c→0</sub> vs q<sup>2</sup>, and [KC/R<sub>vv</sub>(θ)]<sub>θ→0</sub> vs C. The radius of gyration increases with the increase in molar mass. The positive values of A<sub>2</sub> indicate that THF is reasonably good solvent for polymer under study at 25 °C. The values of A<sub>2</sub> decrease as the molar mass increases. This is understandable as the polymer chain increases then the solvent quality become poorer.

The GPC analysis of the products is presented in Table 6. From the Study of Table 6, it could be inferred that the

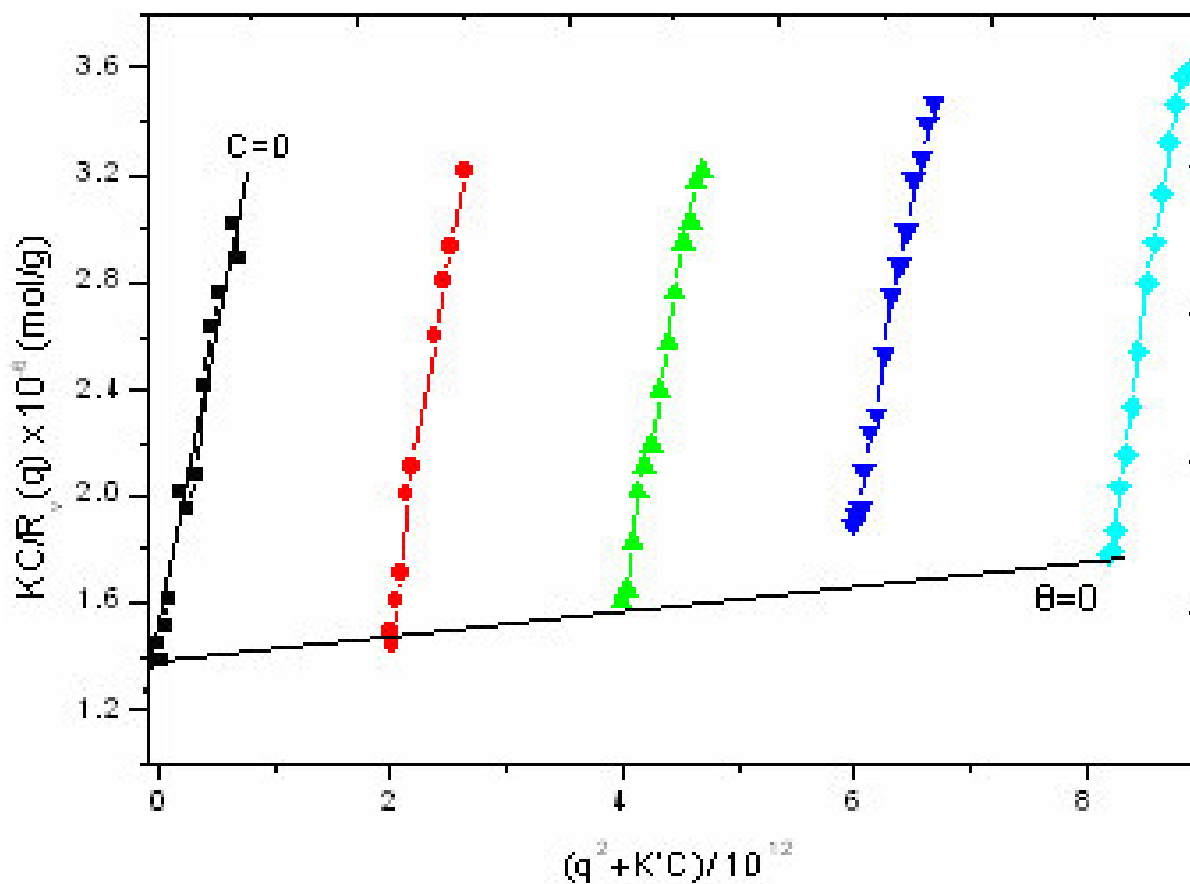


**Figure 10.** Typical zimm plot for the sample calcines at 1173K in THF at 25°C, where the solution was clarified by 0.45  $\mu\text{m}$  filters and C ranged from  $2.0 \times 10^{-3}$  to  $8.00 \times 10^{-3}$  g/ml.

polydispersity is quite narrow of the butadiene products which is supported by variation in chain length.

### Kinetics of butadiene polymerization

The kinetics scheme in polymerization process can handle anionic, cationic, and group transfer polymerization. We proposed here on the basis of our characterization results, the following polymerization scheme: i) Initiator Dissociation; ii) Chain Initiation; iii) Propagation; iv) Association; v) Coupling (with the formation of chain growth intermediate).

The whole polymerization process keeps track of different types of active sites. Once it is dissociated activation and initiation reactions, exchange reaction, chain transfer reaction and chain termination reaction proceeds. We assumed that the associated polymeric species exist as a dimer when butadiene are attached to the catalyst active sites, electronic interaction comes into effect, thus modifying the overall geometry of the

system. In this study we assume that there is only one type of propagating species that is, only ion pair active catalyst sites generated due to different oxidation states of Ni and Co.

Lee et al. (2006) and Hsieh et al. (1996) have extensively studied the polymerization of styrene and butadiene in hydrocarbon solvent using different initiators and solvents. They have reported monomer reactivity ratios in various solvents. Their studies indicate that in polymerization, the reactivity ratios are a strong function of solvent and initiator. For styrene and butadiene the reactivity ratio for butadiene is about 50 times larger than reactivity ratio of styrene in cyclohexane solvent and of course with initiator. In the present study the polymerization reactivity has been achieved by just controlling the particle geometry in the bulk and on the surface which in turn control the equilibrium of the reaction. The percentages of polymer chain are associated in the dimeric nature of associated polymer. In the present study the control of this dimeric nature of chain propagation directs our reaction towards the formation of aliphatic and aro-

matic polymers.

## Conclusion

The bimetallic Ni;Co(ox) catalyst calcined at 1173 K is active for the polymerization of Butadiene. The calcinations temperature of the catalyst produces crystallinity and shifts it towards the multiple phase transition that is, responsible for the increase of active sites. No effect of pressure and temperature was observed on the product distribution. The catalyst active sites geometry and reaction conditions control, product selectivity either towards the formation of aliphatic or aromatic compound.

The characterization results indicate the formation of two types of intermediate, responsible for shifting the product selectivity towards aliphatic or aromatic polymers formation. The nature of acid catalytic active sites controls the catalytic reaction stoichiometry. The polymerization product has very good polydispersity and high molecular weight. The Ni:Co[O<sub>x</sub>] catalyst calcined at 1173 K showed higher activity and selectivity towards polymerization of butadiene in comparison with other catalysts samples in ethanol solvent.

## ACKNOWLEDGMENT

Higher Education Commission, Islamabad, Pakistan research grant no. 20-623/R and D/2519 is for this project gratefully acknowledged.

## REFERENCES

- Barbotin F, Spitz R, Boisson C (1999). Polymerization of butadiene with a new catalyst based on a neodymium amide precursor. *Macromol. Chem. Phys.* 200: 1163-1165.
- Bianchini D, Bichinho KM, dos Santos JHZ (2002). Polyethylenes produced with zirconocene immobilized on MAO-modified silicas. *Polymer* 43: 2937-2941.
- Billmeyer FW (1984). *Polymer Science*, Wiley-Interscience, New York, pp. 96-110.
- Boor IJ (1979). *Ziegler Natta Catalysis and Polymerization*. Academic, New York pp 21-35.
- Brandolini AJ, Hills DD(2000). *NMR Spectra of Polymers and Polymer Additives*. Marcel Dekker, New York pp 123-150.
- Cesteros Y, Salagre P, Medina F, Sueiras JE (2000). *Appl. Catal. B-Environ.* Synthesis and characterization of several Ni/NiAl<sub>2</sub>O<sub>4</sub> catalysts active for the 1,2,4-trichlorobenzene hydrodechlorination 25: 213-215.
- Chu B (1991). *Laser Light Scattering*. Academic Press, New York pp. 335-365.
- Denis VS, Vladimir AZ, Alexander GP, Gennady DB (2009). Supported Ziegler–Natta catalysts for propylene polymerization. Study of surface species formed at interaction of electron donors and TiCl<sub>4</sub> with activated MgCl<sub>2</sub> (In press).
- Dong W, Masuda T (2002). Novel neodymium (III) isopropoxide-methylaluminoxane catalyst for isoprene polymerization. *J. Polym. Sci. Pol. Chem.* 40: 1838-1842.
- Dong W, Masuda T (2003). Homogeneous neodymium isopropoxide/modified methylaluminoxane catalyst for isoprene polymerization. *Polymer* 44: 1561-1563.
- Duan H, Lin X, Liu G, Xu L, Li F (2009). *J. Mater Process Tech.* (In Press).
- Duvakina NV, Monakov YB (2002). Unusual Influence of the Preparation Conditions of Neodymium–Magnesium Catalyst Systems on Their Stereospecificity in Butadiene Polymerization. *Dokl Chem.* 384: 129-135.
- Galvin ME, Heffner SA (1989). Reaction of butadiene with a heterogeneous Ziegler-Natta catalyst in solid polymers and solutions. *Macromolecules* 22: 3307-3313.
- Gilbert RG, Napper DH (1983). The Direct Determination of Kinetic Parameters in Emulsion Polymerization Systems. *Polym. Rev.* 23: 127-131.
- Grieken RV, Calleja G, Serrano D, Martos C, Melgares A, Saurez I (2003). The Role of the Hydroxyl Groups on the Silica Surface When Supporting Metallocene/MAO Catalysts. *Polym. React. Eng.* 11: 17-20.
- Hsieh HL, Quirk RP (1996). *Anionic Polymerization: Principle and Practice*. Marcel Dekker, New York pp 321-330.
- Huang R, Liu D, Wang S, Mao B (2004). Spherical MgCl<sub>2</sub> Supported Iron Catalyst for Ethylene Polymerization: Effect of the Preparation Procedure on Catalyst Activity and the Morphology of Polyethylene Particles. *Macromol. Chem. Phys.* 205: 966-968.
- Huang YJ, Qi GR, Chen LS (2003). Effects of morphology and composition on catalytic performance of double metal cyanide complex catalyst. *Appl. Catal. A-Gen.* 240:263-268. Jin SH, Kim SH, Cho HN, Choi SK (1991). Synthesis and characterization of side-chain liquid-crystalline polymers containing a poly(1,6-heptadiyne) derivative. *Macromolecules* 24: 6050-6055.
- Knoke S, Chem D, Ferrari D, Tesche B, Fink G (2003). Microkinetic. Kowalski G, Pielichowski J, Jasieniak M (2003). Polymer supported cobalt(II) catalysts for alkene epoxidation *Appl. Catal.* 247: 295-302.
- Krajewski-Bertrand M, Laupretre F (1996). <sup>13</sup>C NMR Investigation of the Size of the Moving Units in Polybutadienes of Various Microstructures *Macromolecules* 29: 7616-7618.
- Lee JH, Liu ST (2006). Ethylene Polymerization Catalyzed by Diimine-Palladium (II) Complexes Modified on Silicas. *J. Chin. Chem. Soc.* 53: 1349-1354.
- Mello IL, Coutinho FMB, Nunes DSS, Soares BG, Costa MAS, de Santa Maria LC (2004). Solvent effect in *cis*-1,4 polymerization of 1,3-butadiene by a catalyst based on neodymium, *Eur. Polym. J.* 40: 635-641.
- Mihir MP, Malav AK, Jayantilal DJ (2009). Thermal and catalytic aspects of Ln(III) polymer-metal complexes. *Polym. Int.* 58: 728-731.
- Minhas RK, Scoles L, Wong S, Gambarotta S *Organometallics* (1996). Tri- and Tetravalent Titanium Alkyls Supported by Organic Amides. 15: 1113-1115.
- Monteil V, Spitz R, Boisson C (2004). Polymerization of butadiene and copolymerization of butadiene with styrene using neodymium amide catalysts. *Polym. Int.* 53: 576-578.
- Narayan RV, Kanniah V, Dhathathreyan A (2006). *J Chem Sci*, Tuning size and catalytic activity of nano-clusters of cobalt oxide 118: 179-181.
- O'Connor AR, White PS, Brookhart M (2007). The Mechanism of Polymerization of Butadiene by "Ligand-Free" Nickel(II) Complexes. *J. Am. Chem. Soc.* 129: 4142-4143.
- Pecora R, Berne J1 (1976). *Dynamic light Scattering*. plenum press, New York pp 550-564.
- Penczek S (2002). Terminology of kinetics, thermodynamics, and mechanisms of polymerization. *J. Polym. Sci. Pol. Chem.* 40: 1665-1668.
- Ricci G, Boffa G, Porri L (1986). Polymerization of 1,3-dialkenes with neodymium catalysts. Some remarks on the influence of the solvent, *Macromol. Chem. Rapid. Commun.* 7: 355-360.
- Saltman WM (1977). *The Stereo Rubbers*. Wiley-interscience, New York pp 211-236.
- Sarasua JR, Rodríguez NL, Arraiza AL, Meaurio E (2005). Stereoselective Crystallization and Specific Interactions in Polyactides. *Macromolecules* 38: 8362-8365.
- Serra M, Salagre P, Cesteros Y, Medina F, Sueiras JE (2000). Study of preparation conditions of NiO–MgO systems to control the morphology and particle size of the NiO phase, *Solid State Ionics* 134: 229-231.

- Song IK, Young LW (2003). Heteropolyacid (HPA)-polymer composite films as heterogeneous catalysts and catalytic membranes. *Appl. Catal. A-Gen.* 256: 77-98.
- Takehira K, Shishido T, Wang P, Kosaka T, Takaki K (2004). Autothermal reforming of CH<sub>4</sub> over supported Ni catalysts prepared from Mg-Al hydrotalcite-like anionic clay. *J. Catal.* 221: 43-47.
- Taniguchi Y, Dong W, Katsumata T, Shiotsuki M, Masuda T (2005). *Polym Bull.* Novel Neodymium-Based Ternary Catalyst, Nd(O-*i*-Pr)<sub>3</sub>/[HNMe<sub>2</sub>Ph]<sup>+</sup>[B(C<sub>6</sub>F<sub>5</sub>)<sub>4</sub>]<sup>-</sup>/*i*-Bu<sub>3</sub>Al, for Isoprene Polymerization, 54:173
- Taube R, Sylvester G, Cornils B, Herrmann WA (1996). *Applied Homogeneous Catalysis with Organometallic Compounds.* VCH, Weinheim pp. 280-295.
- Thomas JM, Richard C, Catlow A, Sankar G (2002). Determining the structure of active sites, transition states and intermediates in heterogeneously catalysed reactions. *Chem Commun.* (24): 2921-2925.
- Toshima N, Hirakawa K (1997). Polymer-protected Pt/Ru bimetallic cluster catalysts for visible-light-induced hydrogen generation from water and electron transfer dynamics. *Appl. Surf. Sci.* 121: 534-537.
- Videomicroscopic Analysis of Olefin Polymerization with a Supported Metallocene Catalyst. *Communication* 42: 5090-5093.
- Wilson DJ (1996). Polymerization of 1,3-butadiene using aluminoxane-based Nd-carboxylate catalysts. *Polym. Int.* 39: 235-238.
- Wu C, Xia KQ (1994). Incorporation of a differential refractometer into a laser light-scattering spectrometer. *Rev. Sci. Instrum.* 65: 587-590.
- Xu RW, Liu DB, Wang S, Mao BQ (2006). Preparation of Spherical MgCl<sub>2</sub>-Supported Late-Transition Metal Catalysts for Ethylene Polymerization. *Macromol. Chem. Phys.* 207: 779-781.
- Yu G, Li Y, Qu Y, Li X (1993). Synthesis and characterization of polymer-supported lanthanide complexes and butadiene polymerization based on them. *Macromolecules* 26: 6702-6708.
- Zimm BH (1948). Apparatus and Methods for Measurement and Interpretation of the Angular Variation of Light Scattering; Preliminary Results on Polystyrene Solutions. *J. Chem. Phys.* 16: 1099-2011.